Numerical investigation of CSP air cooled condenser fan

Lorenzo Tieghi[*,1], *Giovanni* Delibra[1], *Alessandro* Corsini[1] and *Johan* Van Der Spuy[2]

[1]Department of Mechanical and Aerospace Engineering, Sapienza University of Rome, Via Eudossiana 18, 00184 Rome, Italy

[2]Stellenbosch University, Private Bag X1, Matieland, 7602, Stellenbosch, South Africa

1 Introduction

CSP power plants are usually installed in desert regions due to the high availability of direct normal irradiance during the year. This usually entails the unavailability of water to be used for condensation in Rankine cycle and the consequent choice of air-cooled condensers (ACCs) [1].

When dealing with ACCs the main mechanical component is the fan, that drives fresh air towards the heat exchangers driving all the process. The main characteristic of this fan is its size that spans from 7 to 13 m of external diameters, thus resulting in a series of technical problems to be addressed. Such high-volume and low speed fans present critical problem during the testing phase [2]. This dissertation focuses on the certification of fan performance, that follows ISO 5801 [3].

Given the size of the actual ACC fan, it is not possible to test it in its full-size, but scaling of the device is required to fit it to smaller facilities, like the Stellenbosh laboratory that was used in this case, where the maximum diameter is fixed at 1.5 m. This of course poses some problems when scaling performance (previous works [4] showed that the scaled performance fits quite well the full size pressure ratio, whilst underestimating efficiency). Another issue in this case is the derating of performance from ISO to real-life installation layout, that is a key issue like in most fan installations. In the following a series of CFD simulations is performed to address this issue and calculate the characteristic curve of the fan in real life installation setup. The setup that is reproduced here is the test-facility for ACCs that was built in Stellenbosh University under Minwater CSP H2020 project [5].

2 CPS test facility description

The simulated geometry reproduces a CSP test facility that is currently installed at the Stellenbosh University, South-Africa. The experimental apparatus is designed to reproduce a full-size A-Type air cooled condenser [6]. The geometry is sketched in Figure 1: the fan (5) forces an air flow from

---

[*] Corresponding author: lorenzo.tieghi@uniroma1.it

the atmosphere (1) to the exchanger chamber (3). The air serves as the cooling fluid to condensate steam, flowing across a tube bundle (not shown). In this configuration a squared grid is present upstream the tubes and acts as pavement for operators (4). The fan design and operative parameters are summarized in Table 1.
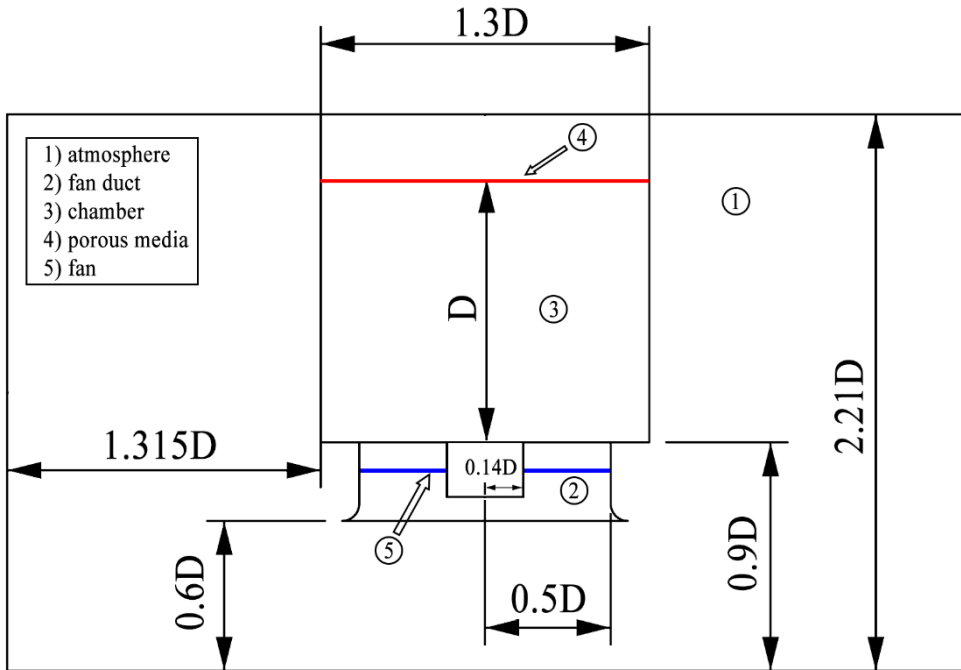

Figure 1 – experimental apparatus geometry

Table 1 – Design and operative parameters of the fan

Geometrical Parameters	Value	Operative Parameters	Value
Fan diameter	7.373 m	Mass flow rate	333 m³/s
Hub to tip ratio	0.284	Rotational speed	151 rpm
Tip clearance	0.369 m	Expected total to static pressure rise	105 Pa
Number of blades	8	Expected static efficiency	61 %
Hub to tip ratio	0.29	Air temperature	298.15 K

3 Numerical Methodology

The steady RNG k-ε simulations were carried out using OpenFOAM – v2.3, using the *porousSimpleFoam* solver. The RNG k-ε model improves the standard k-ε model formulation, by a better computation of turbulent diffusivity [7]. The RNG model is suited for the simulation of incompressible rotating flows. It To reduce the computational costs of the simulations, the fan and the grid are modelled using an Actuator Disk Model (ADM) and a porous media, respectively.

3.1 Computational grid and boundary conditions

The experimental apparatus is discretized using a three-dimensional domain that entails 5M hexahedral cells. The cell wall spacing is set to achieve a y^+ value of 30 on all the solid surfaces. Two *Arbitrary Mesh Interfaces* (AMIs) represent boundary the exterior / interior of the chamber and the rotor region, Figure 2. A constant mass flow rate, equal to 1/4 of the nominal mass flow rate of the fan, is imposed on all the lateral boundaries. The inlet turbulent intensity is set to 1%, and dissipation length follows accordingly. The upper boundary of the domain is treated as a slip surface. The lower boundary, corresponding to the terrain, is treated using a neutral atmospheric boundary layer model. No-slip boundary conditions are imposed at the solid walls for velocity, where k and ε rely on the standard wall functions. The outlet of the exchanger chamber is treated using zero gradient boundary conditions. A zero gradient boundary condition is applied to the pressure on all the boundaries.

Figure 2 – Fan region scheme (left) and computational grid (right).

3.2 Porous media model

The 20-mm thick grid is characterized by squared holes with a size 50 mm. Such grid is responsible of a static pressure loss of 40 Pa at the nominal mass flow rate (Q = 333 m³/s). The fluid dynamic losses were estimated according to the methodology highlighted in [8]. The resistance curve of the grid was used to design the porous media, deriving the coefficients of the well-known Darcy-Forchheimmer equation:

$$\frac{\partial p}{\partial x} = -\frac{\mu}{\kappa}Q - \frac{\mu}{\kappa_1}Q^2 \tag{1}$$

3.3 Actuator Disk Model (ADM)

The effect of the momentum exchange between the fan blades and the air was simulated using an in-house Actuator Disk Model [9]. The model adds a source term f_i into momentum equation, corresponding to:

$$f_i = \frac{1}{2}W_\infty^2 \sigma F_i \frac{1}{\Delta z} = \left[\frac{1}{2}W_\infty^2 \sigma (C_L + C_D)\frac{1}{\Delta z}\right]\hat{\imath} \tag{2}$$

where i denotes the axial direction.

3.4 Numerical schemes

The stationary numerical simulations relied on simpleFoam incompressible solver. The Generalized Algebraic Multi-Grid solver (GAMG) was used for pressure and *smoothSolver* for the other equations. The simulations ran until the full convergence of the flow fields, with the thresholds set to 10^{-9} and 10^{-7} for pressure and the other quantities, respectively.

4 Results

This section reports the results as a function of three different mass flow rates, 320 – 333 and 346 m^3/s respectively. During the design process, the installation losses are usually not considered. In fact, in most cases it is not possible to preliminary assess the effect of the installation setup on the turbomachinery flow. To this extent, the effect of the installation through a visualization of the characteristic curve of the fan (Figure 3) is first evaluated. The total to static pressure (TTS) is measured as the pressure delta between the inlet and the outlet of the duct and the dynamic pressure at the inlet. The rotor-only numerical data are available from [10].

Table 2 – TTS pressure, ACC vs rotor only

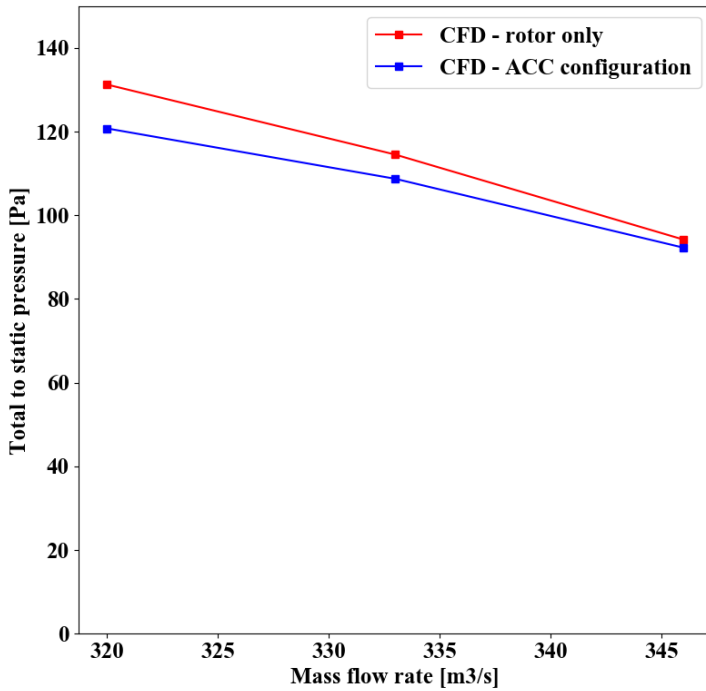| Mass flow rate [m^3/s]	Total to static pressure [Pa]	
	ACC configuration	Rotor only
320	120.76	131.25
333	108.7	114.5
346	92.26	94.2

Figure 3 – Comparison between TTS pressure, rotor only CFD (solid red line) vs installation CFD (solid blue line)

As expected, the installation of the fan leads to a loss in static pressure. At 320 m^3/s, a 1% loss in the TTS pressure (Table 2) is observed. However, the effect becomes less evident while moving along the characteristic curve, and losses can be almost neglected at the highest flow rate, where it exerts a 2 Pa loss with respect to the ISO installation. It is possible to conclude that, depending on the duty point, the installation of the fan can have a mild impact on the efficiency of the fan, and such aspect should be ideally taken in account during the design process. The flow field is characterized by a strong recirculation given by the high diameter of the hub, that behaves as a bluff body. The pressure loss downstream of the fan hub is the trace of the Von Karman vortices that are released as function of the rotational speed of the fan. Such aspect has been investigated through a transient simulation of the flow (not reported in the manuscript).
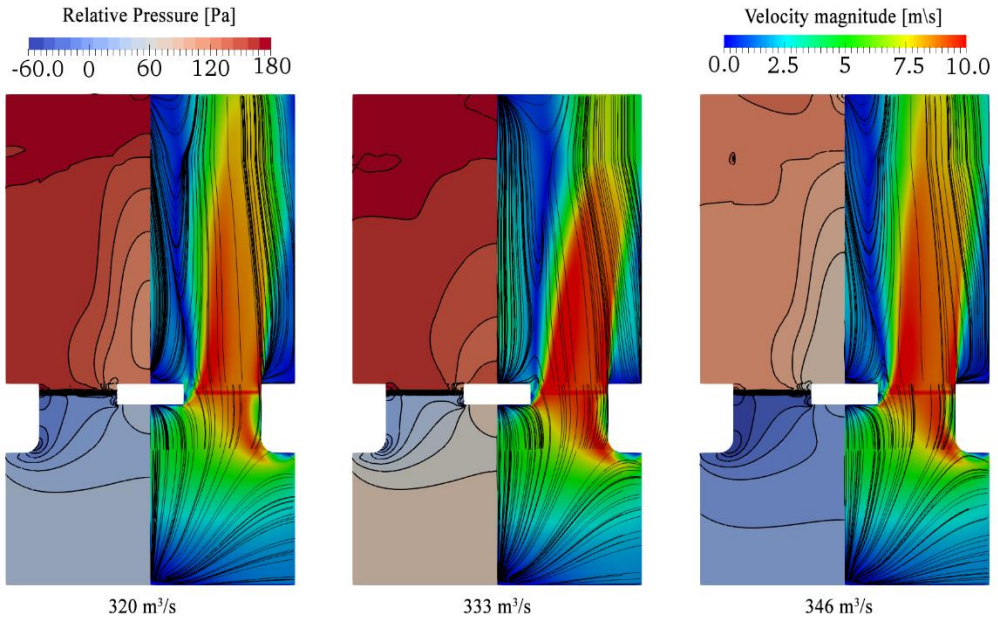
Figure 4- Relative pressure contour and velocity streamlines as a function of the mass flow rate

The unsteadiness of the flow is enhanced by two factors: the sharp edges of the rotor disk (a spinner cone is not present in the experimental setup) and by the fan geometry itself. In fact, as evident further in the text, the fan is designed to work from the midspan of the blade, whereas the fan sections that are closer to the hub exert a structural function only. It leads to a flow separation at the hub, more marked at the higher flow rates, that is amplified downstream of the rotor disk. Such behaviour could not be observed by the sole simulation of the rotor. The evident discontinuity in the pressure field in Figure 4 is caused by the actuator disk model, that is also responsible of the higher local flow velocity. The straightening of the flow, close to exit of the chamber downstream of the fan, is caused by the porous media that replicates the presence of the grid. The worsening in the specific work of the fan can be further analysed by looking at the β_1 and β_2 angle distributions. Figure 5 shows that there is a good match between the design hypothesis and the numerical results in term of inflow angle, for most of the span of the blade. However, the biggest differences can be found in the hub region, approximately for the first 20% of the blade span, where the flow separation pointed out by numerical simulations is not taken in account in the design phase. Up to the 15 % of the blade span, the fan is working as a turbine, as it is absorbing work from the fluid (Figure 6). A deeper analysis of the fan behaviour can be achieved by looking at the velocity profiles in Figure 7.
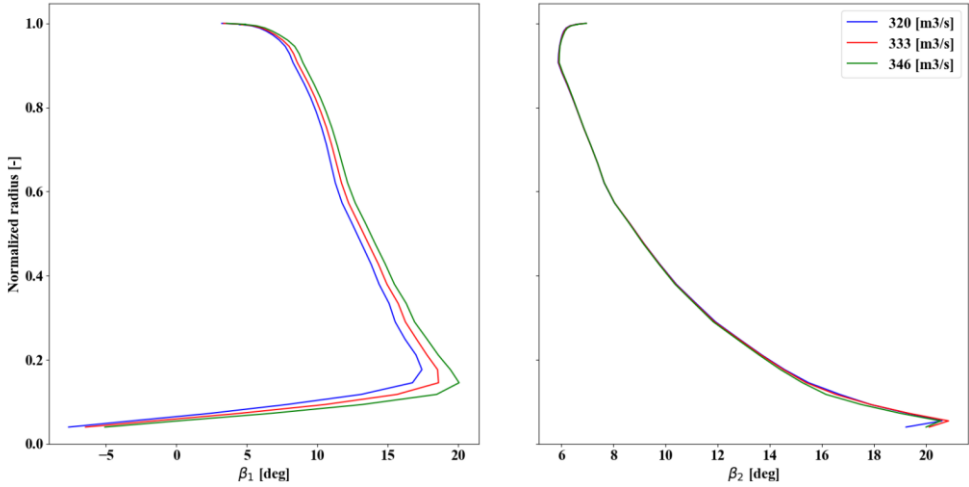
Figure 5 – Inflow (left) and outflow (right) relative flows angles, as a function of the flow rate

The fan is working close to the design assumptions for most of the blade span, whereas the strong deflections that can be seen close to the hub of the blade exerts that the recirculating flow is seriously impairing the correct fan design. The presence of the recirculation at the hub of the fan is evident from the axial velocity profiles, where a negative velocity equal to 20% of the bulk velocity is observed. The amplitude of the recirculating area affects almost the 20 % of the blade span in the worst scenario (320 m^3/s), whereas the minimum amplitude is found at the nominal mass flow rate (red line).
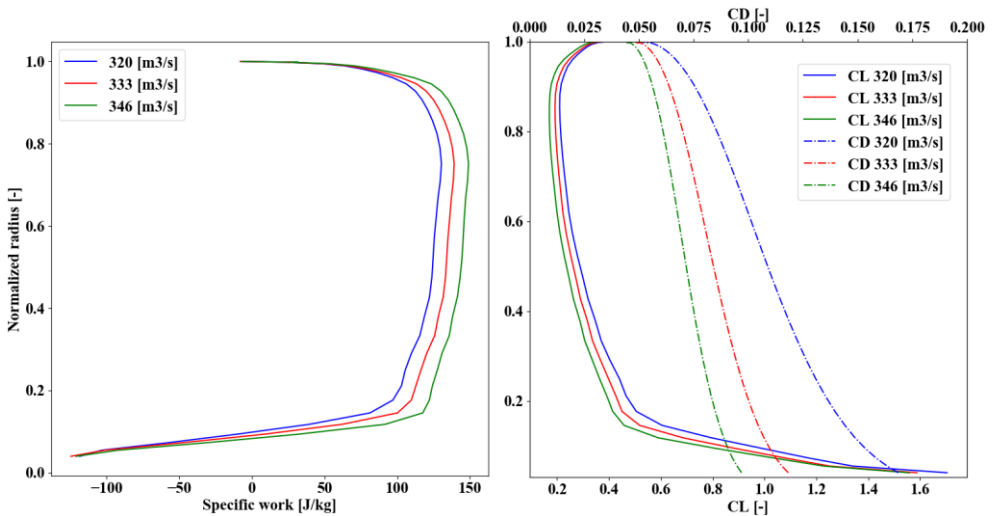

Figure 6 – Specific work (left) and lift/drag coefficients (right) distributions as a function of the mass flow rate

The presence of the recirculating flow is reflected on the radial velocity, where the maximum radial velocity is comprised between the 10% and the 20% of the blade span, that can locally reach up to the 50% of the bulk velocity (at the design mass flow rate). In the first 5 % of the blade span also report a negative radial velocity is found. The tangential velocity distribution reflects the mixed vortex assumption, assumed during the design phase of the fan.
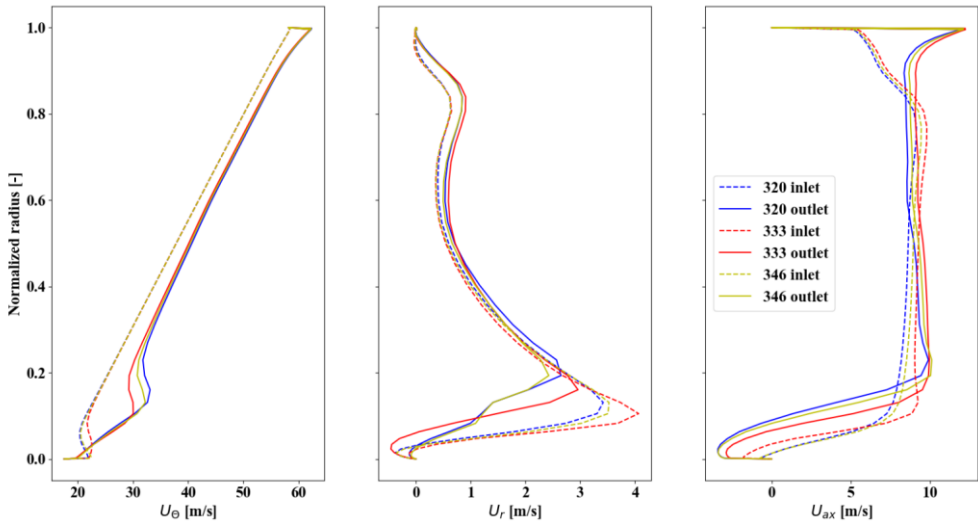

Figure 7 - left to right: tangential, radial and axial inlet and outlet velocities as a function of the mass flow rate

5 Conclusions

The combination of porous media and synthetic blade modelling has allowed an accurate numerical simulation with reasonable computational costs. It is possible to draw two main conclusions.

First, the numerical simulations point out how, during the design phase of the fan, the final installation of the turbomachinery may lead to strong deviation from the design parameters. Such aspect can be also easily extended to the validation of a design, where traditional CFD rotor-only methods do not take in account flow deflections that can be attributed to the setup. In this case, the fan characteristic curve, obtained from the full numerical simulations of the experimental apparatus, exerts some deflections from the rotor only CFD previously obtained. This is particularly marked at the lowest mass flow rate where the fan shows a 10 Pa TTS pressure loss, with respect to the rotor-only simulation. The cause of such derating was found in the rotor disk design.

In fact, by looking at the velocity and pressure fields, the role of the rotor disk in perturbating the air flow is highlighted. In this case, the absence of a spinner cone has made the rotor disk to act as a blunt body, with the release

of huge vortices downstream of the fan. In addition, it has led to a separation of the flow close to the hub, where the blade is working in off-design condition.

To conclude, this installation may obtain great benefit from the installation of a properly designed spinner cone upstream of the fan, neglecting the recirculating flows at the inlet of the fan.

References

1. Fay, H. P. (1997). U.S. Patent No. 5,632,329. Washington, DC: U.S. Patent and Trademark Office.
2. Kammel, D. W., & Kappelman, J. J. (2003). Design of high volume low speed fan supplemental cooling system in dairy free stall barns. In Fifth International Dairy Housing Conference for 2003 (p. 243). American Society of Agricultural and Biological Engineers. DOI:10.13031/2013.11628
3. ISO 5801, 2007, 'Industrial Fans – Performance Testing using Standardized Airways'.
4. Wilkinson, M., van der Spuy, J., and von Backström, T. The Design of a Large Diameter Axial Flow Fan for Air-Cooled Heat Exchanger Applications. Proceedings of the ASME Turbo Expo 2017. DOI:10.1115/GT2017-63331.
5. The MinWaterCSP Project - http://www.minwatercsp.eu/minwatercsp_project/ 2017.
6. Kirstein, C., von Backström, T. and Kröger, D. (2005). Flow Through a Solar Chimney Power Plant Collector-to-Chimney Transition Section. International Solar Energy Conference. DOI: 10.1115/ISEC2005-76011.
7. Yakhot, V., Orszag, S.A., Thangam, S., Gatski, T., and Speziale, C.G. (1992). Development of turbulence models for shear flows by a double expansion technique. Physics of Fluids, 4, 1510-1520. DOI:10.1063/1.858424.
8. Idelchik, Isaak E. "Handbook of hydraulic resistance." *wdch* (1986)
9. Bonanni, T., Corsini, A., Delibra, G., and Volponi, D. (2017). Development and Validation of a Novel Synthetic Blade Model for Axial Flow Fans in Unsteady CFD. V001T09A005. DOI:10.1115/GT2017-63952.
10. Volponi, D., Bonanni, T., Tieghi, L., Delibra, G., Wilkinson, M., van der Spuy, J. and von Backström, T. (2018). CFD Simulation Results for the MinWaterCSP Cooling Fan. DOI: 10.13140/RG.2.2.22031.89768.